*12082–12093* *Nucleic Acids Research, 2022, Vol. 50, No. 21* *Published online 7 December 2022*
*https://doi.org/10.1093/nar/gkac1113*

# Displacement and dissociation of oligonucleotides during DNA hairpin closure under strain

**Fangyuan Ding [1,2,3,*], Simona Cocco[4], Saurabh Raj[5], Maria Manosas[6,7], Thao Thi Thu Nguyen[2], Michelle M. Spiering[8], David Bensimon[4,9,10], Jean-François Allemand[4,9] and Vincent Croquette[4,9,11,*]**

[1]Department of Biomedical Engineering, University of California, Irvine, CA 92617, USA, [2]Center for Complex Biological Systems, University of California, Irvine, CA 92697, USA, [3]Center for Synthetic Biology, Chao Family Comprehensive Cancer Center, Department of Developmental and Cell Biology, and Department of Pharmaceutical Sciences, University of California, Irvine, CA 92697, USA, [4]Laboratoire de Physique de l'Ecole normale supérieure, ENS, Université PSL, CNRS, Sorbonne Université, Université Paris Cité, Paris, France, [5]Kusuma School of Biological Sciences, Indian Institute of Technology, Delhi, 110016, India, [6]Small Biosystems Lab, Departament de Física de la Matèria Condensada, Facultat de Física, Universitat de Barcelona, Carrer de Martí i Franquès, 1, 08028 Barcelona, Spain, [7]Institut de Nanociència i Nanotecnologia (IN2UB), Universitat de Barcelona, 08028 Barcelona, Spain, [8]Department of Chemistry, The Pennsylvania State University, University Park, PA 16802, USA, [9]Institut de Biologie de l'École Normale Supérieure (IBENS), CNRS, Inserm, École Normale Supérieure, PSL Research University, F-75005, Paris, France, [10]Department of Chemistry and Biochemistry, University of California Los Angeles, Los Angeles, CA 90095, USA and [11]ESPCI Paris, Université PSL, Paris, France

Received June 20, 2022; Revised October 19, 2022; Editorial Decision November 01, 2022; Accepted November 07, 2022

## ABSTRACT

**The hybridization kinetic of an oligonucleotide to its template is a fundamental step in many biological processes such as replication arrest, CRISPR recognition, DNA sequencing, DNA origami, etc. Although single kinetic descriptions exist for special cases of this problem, there are no simple general prediction schemes. In this work, we have measured experimentally, with no fluorescent labelling, the displacement of an oligonucleotide from its substrate in two situations: one corresponding to oligonucleotide binding/unbinding on ssDNA and one in which the oligonucleotide is displaced by the refolding of a dsDNA fork. In this second situation, the fork is expelling the oligonucleotide thus significantly reducing its residence time. To account for our data in these two situations, we have constructed a mathematical model, based on the known nearest neighbour dinucleotide free energies, and provided a good estimate of the residence times of different oligonucleotides (DNA, RNA, LNA) of various lengths in different experimental conditions (force, temperature, buffer conditions, presence of mismatches, etc.). This study provides a foundation for the dynamics of oligonucleotide displacement, a process of importance in numerous biological and bioengineering contexts.**

## INTRODUCTION

DNA hybridization is pervasive. It mainly happens under two general schemes: (1) oligonucleotides freely binding/unbinding on a ssDNA template or (2) competition between oligonucleotides on a DNA template. Both schemes play significant roles in fundamental biology. The free-binding configuration is known to be the foundation of base-pairing recognition, and the competitive configuration plays a role in various biological conditions. During replication arrest (Supplementary Figure S1a), an oligo-hybrid can be displaced by the receding fork, creating a structure known as a chicken foot that must be separately processed before replication can restart. Similarly, during transcription (Supplementary Figure S1b), the competition between the DNA fork ahead of the transcription bubble and the DNA/RNA hybrid behind it may result in transcriptional pausing (1). The competition between a fork and an adjacent hybrid has also been used in many practical applications, such as Hybridization Chain Reaction (HCR) (2), DNA walker (3), DNA Origami (4,5), DNA sequencing (6), and a genomic DNA editing technology (7), known

*To whom correspondence should be addressed. Tel: +1 949 824 1813; Email: dingfy@uci.edu
Correspondence may also be addressed to Vincent Croquette. Email: vincent.croquette@lps.ens.fr

as Clustered Regularly Interspaced Short Palindromic Repeats (CRISPR) (Supplementary Figure S1c). CRISPR appears to rely on the opening of the DNA helix and the displacement of the forks by a complementary guide RNA oligonucleotide. In that instance, the efficiency and specificity of recognition and editing depend on the existence of mismatches between the guide RNA and the target DNA strands that might favor the displacement of the hybrid by the DNA fork(s). The competition and replacement of proteins bound on DNA is a similar process, which has been investigated in single molecule experiments (8,9). It is thus important to characterize both hybridization configurations. To simplify the description, from now on, we refer to the free-binding situation as the 'dissociation' scheme and the competitive situation as the 'displacement' scheme.

Previous studies have elucidated many aspects of the dissociation scheme. By using nearest neighbour free energies (10–12), one can accurately predict many equilibrium thermodynamic parameters, such as the melting temperature $T_m$ and affinity constant $K_d$. However, in many biological situations, the important parameter determining the occurrence of a reaction is the lifetime of a hybridized state but not its $K_d$. Characterizing kinetic parameters, such as the hybridization lifetime $\tau_{off}$ or the binding time $\tau_{on}$, requires capturing the dynamic process of hybridization. Although fluorescent-based techniques (such as FRET (13)) have been used to investigate the kinetic parameters, data throughput is relatively low due to the complexity of the experimental design, and the fluorescent labelling may affect the hybridization dynamics. Similarly, the kinetic parameters of the 'displacement' scheme remain poorly investigated due to technical difficulties in capturing real-time oligonucleotide competition.

In this paper, we propose a label-free platform to quantify the kinetic parameters for both schemes. Specifically, we used a magnetic trap to pull on a DNA hairpin. At a large enough tension, the hairpin is unzipped (6,14) and the resulting ssDNA strand can hybridize with oligonucleotides in solution. As the tension on the molecule is reduced, the hairpin refolds but the DNA fork may be blocked transiently by the presence of these oligo-hybrids in the refolding pathway. With an oligonucleotide complementary to the hairpin stem, we characterized the 'displacement' kinetics by studying the blockage times during refolding. Namely, the displacement times, $\tau_{disp}$, of blocking oligo-hybrids by the receding fork as a function of force, temperature, length, and type of oligonucleotide (e.g. RNA, or Locked Nucleic Acid (LNA), mismatches, etc.). Similarly, by using an oligonucleotide complementary to the hairpin apex, we characterized the dissociation kinetics by studying the time lag required for hairpin nucleation and refolding upon tension release.

We found that the dissociation kinetics are consistent with the standard oligonucleotide hybridization estimates, whereas the measured 'displacement' times are much shorter than the 'dissociation' times due to competition from the adjacent DNA from the hairpin. Additionally, at low forces, we observed that the existence of complementary sequences flanking the oligonucleotide allows for the possibility of encirclement reducing the blockage lifetime for hairpin nucleation and refolding.

We propose a model valid for the description of both displacement and dissociation schemes. By using the known free energies of hybridization between (complementary or non-complementary) bases, our model fits all the experimental data with a few adjustable parameters. It is straightforward to exclude the displacement by the fork, thus providing a tool to predict simple oligonucleotide dissociation. Finally, by including the encircling mechanism in this model, we can describe the dissociation dynamics of an oligonucleotide blocking a loop. We also performed a stringent test of the model, sorting out the importance of various physical parameters, such as salt concentrations, by using an extra controlled variable (the tension on the fork). Together, this theoretical framework provides new insights into this pervasive biological process.

## MATERIALS AND METHODS

### Magnetic tweezers

Experiments were done on a commercial PicoTwist magnetic tweezers (www.picotwist.com) with single DNA hairpins tethered between a coverslip via a digoxigenin-anti-digoxigenin bond and a magnetic bead via a biotin-streptavidin bond. DNA molecules were mixed with streptavidin magnetic beads (Dynabeads@ MyOne™ C1, Invitrogen). Then, we gently flowed the mixture into a 5 mm × 40 mm × 40 um pre-coated anti-digoxigenin chamber. After 5–15 min incubation, we rinsed the chamber thoroughly to remove unattached beads/samples. We changed the chamber environment to defined buffer conditions with proper oligonucleotides accordingly. The applied force ($F_{test}$, $F_{open}$) on the hairpin is controlled by varying the distance between a pair of permanent magnets from the sample. The position and extension of the hairpins are monitored through a 30 Hz video-camera (CM-140 GE Jai) and tracked through a self-written program. More details on magnetic tweezers (including flow cell fabrication, sample preparation and molecule manipulation as well as measurement) have been described previously in (6).

### Single molecule assay

Due to the high degree of parallelism of magnetic tweezers, we can simultaneously apply the same force on many single molecules. For every experiment in this paper, we always repeatedly zipped-unzipped molecules > 100 times, deduced the needed value (e.g. $<\tau_{disp}>$, $P_{block}$, etc.) for each molecule, and calculated the variation (i.e. error bars in Figures 2–4 and 6) among different molecules. Unless marked otherwise, all the experiments were performed at room temperature under T4 buffer conditions: 0.2% BSA (Bovine Serum Albumin), 25 mM Tris−Ac, 150 mM KOAc, 10 mM $MgOAc_2$, filtered by 0.22 μm filter. The oligonucleotides were ordered from Eurogentec and Integrated DNA Technologies. The detailed protocol to synthesize 1.2 kb hairpin is described in (15). The preparation method for 83 bp hairpin fellow published methods in (6).

### Oligonucleotide sequence

The sequences of small (<12 nucleotides (nt)) are given in the figures. The sequence of the 37 nt oligonu-

cleotide is: 5′-GGGTGTTTGATTGATTTGATTCCTTG GATGTGCGAAG-3′.

The sequence of the 95 nt oligonucleotide is 5′-TTTGGC TAAATATCCTAATGTTAAAG

TGTATGATAAGCCTACTACAGTAGATTTTG ACGGGTGTTTGATTGATTTGATTCCTTGGATG TGCGAAG-3′.

### Elasticity model for ssDNA, dsDNA and pairing energy parameters

For the stretching energy $g_{ss}(f)$ of a ssDNA base at the force $f$, we use the freely jointed-chain model with monomeric length $b_0 = 1.828$ Å and effective stretching length $d = 0.605$ Å (S1).

For the stretching energy $g_{ds}(f)$ of a dsDNA base pair at the force $f$, we use the Odijk formula (16) for the Worm-Like chain model with stretching corrections (S2) with monomeric length $h = 3.4$ Å, and the persistence length is $\xi = 50$ nm.

### Nearest neighbour parameters

The pairing parameters $g_o\,(n, n+1)$ depend on the base pair and the following one due to stacking effects, and can be decomposed into the enthalpic and entropic contribution: $g_o\,(n, n+1) = \Delta H\,(a_n,a_{n+1}) + T\Delta S\,(a_n,a_{n+1},ic)$, where $a_n$ is the nucleotide in position $n$ on the oligonucleotide (as a comparison, $N$ is the total number of oligonucleotide bases and n is between 0 and N) and $ic$ is the ionic conditions. We have taken the $\Delta H$ and $\Delta S$ parameters from Santa Lucia, see Supplementary Table S1. We have not used any initialization cost but an end destabilization obtained by halving the pairing energy of the last two attached base pairs of the oligonucleotide. Note that we estimate such positions to be at the antepenultimate and penultimate position for the fork blocking assay and to be in the middle one for the case of the loop blocking assay for the two oligonucleotides under study which have a symmetric sequence.

### Dissociation time of the oligonucleotide in the fork-blocking assay

The model, as detailed in Supplementary note 2, is an extension of a zipping model introduced in (17) and is based on a stochastic motion of the opening/closing fronts. Such motion is described by the transition matrix built from the probabilities to open or close a base pair of the oligonucleotide (on one of the two sides) or of the hairpin, until oligonucleotide expulsion.

As described in Figure 5, the probability to open base pairs $n_o$ of the oligonucleotide depends on its pairing and stacking energies, $g_o(n_o, n_o+1)$, ( (18,19) and Supplementary Tables S2 and S3) $r_o{}^o(n_o) = 1/t_o \exp[-g_o\,(n_o, n_o+1)]$, whereas the probability to close a base pair depends only on the force via the single strand and double strand stretching energies, $g_{ss}(F)$ and $g_{ds}(F)$: $r_c{}^o = 1/t_o \exp[-g_{ss}\,(F) - g_{ds}\,(F)]$.The probability to open the base pair $n_h$ for the hairpin is $r_o{}^h\,(n_h) = 1/t_o \exp[-g_o\,(n_h,n_h+1)]$, while the probability to close a base pair is $r_c{}^h = 1/t_o \exp[-2g_{ss}\,(F)]$. The transition matrix is of dimension growing as $N^3$, where $N$ is the number of oligonucleotide base pairs, due to the three possible opening-closing fronts. It is zero for opening-closing transitions on non-adjacent base pairs; it has heterogeneous entries due to the sequence dependence of the pairing energies; moreover, it reflects the fact that closing of a base is not possible if it is already paired with the competing random walk. (See Supplementary note 2 for the detailed description of the transition matrix.)

The average displacement time is computed by the average time spent in all possible configurations in which the oligonucleotide is completely or partially bound to the fork, starting with the initial completely bound oligonucleotide and ending with the dissociated one (happening as soon as only 2 bp (a dinucleotide) remain bound to mimic the presence of an opening fork). As detailed in Supplementary note 2, the displacement time can be numerically computed by the scalar product of the inverse of the transition matrix between the initial configuration and the holding configurations having at least two attached base pairs for the oligonucleotide. Such semi-analytical computation is in very good agreement with Monte-Carlo Simulations (Supplementary note 1 and 3, Figures S3, S4 and S7–S12) of the opening-closing fronts based on the same transition matrix (Supplementary note 2).

The solid lines for $<\tau_{disp}>$ in Figures 2 and 3 are obtained by the semi-analytical ($9 \leq N \leq 37$) or Monte-Carlo simulations ($N = 97$)

The overall dependence on unzipping force, temperature and sequence content can be understood from the free energy barrier estimated for such process. In the standard replacement process, for a complementary DNA oligonucleotide, there is no overall loss of pairing energy. The total cost to replace, by the closing fork, $N$ nucleotides occupied by the oligonucleotide is:

$$\Delta g^r = N\,(g_{ss}\,(F) + g_{ds}\,(F)) \tag{1}$$

we then expect for the Arrhenius law, the exponential decay observed:

$$P\left(\tau_{disp}\right) \approx \exp\left(-\tau_{disp}/\ <\tau_{disp}>\right) \tag{2}$$

where $\ln <\tau_{disp}> \propto \Delta G_{disp}/k_B T$ and $\mathrm{d}(\ln<\tau_{disp}>)/\mathrm{d}F \propto N\,(l_{ds} + l_{ss})/k_B T$, $l_{ds}\,(F)$ and $l_{ss}$ are the double-strand and single strand extension per nucleotide at the force $F$ (Supplementary note 2). Such barrier (1) shown in Figure 1D explains the observed dependence of $<\tau_{disp}>$ on the oligonucleotide length, the possibility to replace very long oligonucleotides by lowering the force $F$, and the small sensitivity to sequence content, ionic condition, and temperature for a standard replacement process. Equation (1) does not hold in presence of mismatch, hybrid bases or RNA in the oligonucleotides. In such cases, there is a change in pairing energy, and the displacement time is very sensitive to all the parameters affecting the pairing energy and to the position of the mismatch.

### Dissociation time of the oligonucleotide in the loop-blocking assay

To calculate the dissociation time of the oligonucleotide in the loop-blocking assay, we model the unpeeling of the oligonucleotide by a stochastic step-by-step unpeeling from

both the 5′ and 3′ ends of the oligonucleotide, with opening rate $r_o^o\ (i) = 1/t_o \exp(-g_o\ (i, i+1))$ and closing rate $r_c^o = 1/t_o \exp(-g_{ds}\ (F) + g_{ss}\ (F))$.

The Arrhenius energy barrier for this process is

$$\Delta g^u = \sum_{n_o=1}^{N} g_0\,(n_o, n_o+1) + N\,(g_{ds}\,(F) - g_{ss}\,(F)) \quad (3)$$

The first term, which does not appear in the replacement energy barrier (Eq. 1), corresponds to the unpairing energy of the oligonucleotide at zero force and is the sum of the $N$ nearest-neighbour pairing parameters $g_0\ (i, i+1)$ (18,20). This contribution is large and explains the high stability of the oligonucleotide: one additional pair in the 9 bp oligonucleotide with respect to the 8 bp oligonucleotide, $g_0\ (G, C) \sim 3\ k_B T$, gives the measured ratio between the unbinding times $e^3 \sim 20$. With the same reasoning, the expected time for a 7 bp oligonucleotide will be in the range of hundreds of milliseconds, in the limit of our detection range. The second contribution to the unpeeling energetic barrier in (Eq. (3)) derives from the non-zero test force and is the difference between the stretching energy of the double-stranded and the single-stranded DNA. Using the Arrhenius description (like in Eq. (2)) we obtain $\mathrm{d}(\ln<\tau_{off}>)/\mathrm{d}F \propto N\ (l_{ds} - l_{ss})/k_B T$.

Such a force behaviour explains the presence of a maximum in $\tau_{off}$ around 5 pN in Figure 4C (where $l_{ds} = l_{ss}$). At $f > 12$ pN, $g_{ds}(F) > g_{ss}(F)$ and the unpeeling is facilitated by the stretching force, but it is still an activated process due to the base-pairing term. Only at very large forces of several tens of pN (40–60 depending on sequences) does the activation barrier disappear (21). As detailed in Supplementary note 2, similarly to the replacement, we have precisely calculated the $\tau_{off}$ of the oligonucleotide using a stochastic base by base unpeeling process occurring from both 3′ and 5′ ends (17).

In the loop-blocking assay description, we have added to the transition matrix an escaping transition through encirclement, depending both on the length of the encircling loop and the force.

To model the escaping rate (See Supplementary note 2), we compute its energetic cost through the encirclement $\Delta g^c$. We suppose that the minimal encircling loop with $n$ hybrid hairpin-oligonucleotide base pairs in the middle is a triangle with $n$ single-strand base pairs on each side of the double strand (see the transition state b) in Figure 4), and we compute the mechanical energy required to shorten the extension of the molecule by such a triangle:

$$\Delta g^c = n\,(g_{ds}\,(F) + 2g_{ss}\,(F))$$

using (Eq. (2)) we obtain $\mathrm{d}(\ln<\tau_{off}>)/\mathrm{d}F \propto n\ (l_{ds} + 2\ l_{ss})/k_B T$.

## RESULTS

### A single molecule assay to study DNA fork blocking

We first focus on the 'displacement' scheme. Our assay is based on the mechanical unzipping of a DNA hairpin with a magnetic trap set-up (Figure 1A). Briefly, a DNA hairpin is used to tether a micron-size magnetic bead to a glass surface. Small permanent magnets are used to pull on the tethered bead and subsequently, above a threshold force, unzip the hairpin. This set-up makes it possible both to control the applied force (via the distance of the magnets to the sample) and to measure the extension of the DNA molecule (by analysing the image of the tethered bead).

In the fork-blocking assay, the DNA hairpin is first unzipped by applying a high force $F_{open}$ (>15 pN). Reducing this force to $F_{test}$ (< 12 pN) allows for a quick refolding of the hairpins (22). Unzipping/re-zipping cycles can be repeated on the same molecule in the presence of a complementary oligonucleotide in solution. Hybridization events lead to transient blockage at $F_{test}$, (see pauses in the extension signal, $Z_{block}$, at level (iii) in Figure 1B and C). $Z_{block}$ reflects the actual position of the hybridized oligonucleotide (oligo-hybrid) on the DNA hairpin (conversion to bp is obtained using ssDNA elasticity as in (23–25)). This opens interesting perspectives for DNA identification and sequencing (6). This configuration is similar to a stalled replication fork.

### Measuring the average displacement time $<\tau_{disp}>$ in the fork-blocking assay

The oligonucleotide displacement time $\tau_{disp}$ is deduced from the statistics and duration of blockages. As shown in Figure 2 (inset), these blockages display a single exponential distribution for $\tau_{disp}$ with a characteristic mean blockage time $<\tau_{disp}>$.

### Effect of the force $F_{test}$, the oligonucleotide length $N$, and temperature $T_{on}$ $<\tau_{disp}>$

The displacement time $<\tau_{disp}>$ increases exponentially with both $F_{test}$ and $N$ (the number of oligonucleotide base pairs) and decreases exponentially with $T$ (see Figure 2), a behaviour consistent with our intuition: increasing $F_{test}$ reduces the stability of the hairpin and its propensity to displace the oligo-hybrid; increasing the number of bases $N$ in the oligo-hybrid increases the number of steps required to displace the oligonucleotide; finally, high temperatures destabilize the oligo-hybrid. The displacement time $<\tau_{disp}>$ is almost independent of the salt concentration (see Supplementary Figure S6).

### Effect of the nature of the oligonucleotide and the presence of hybrid nucleotides and mismatches on $<\tau_{disp}>$

Nucleotides such as RNA, methylated bases, and LNA improve the stability of their hybrid with DNA (20,26) and thus increase $<\tau_{disp}>$: it increases by ∼4 for a 11 nt RNA oligonucleotide (Figure 3A) when compared to the same DNA oligonucleotide; a single LNA base increases $<\tau_{disp}>$ by ∼2, and three LNA bases by ∼10 (Figure 3B); a single methylated cytosine may increase $<\tau_{disp}>$ by ∼1.3 (data not shown).

In contrast, mismatches reduce $<\tau_{disp}>$ in a position-dependent manner (Figure 3C). A mismatch at the first base reduces $<\tau_{disp}>$ by a factor ∼5, and by a larger factor when in the middle of the oligo-hybrid. With two mismatches in the middle of a 12 nt oligonucleotide, blockage is no longer detectable within the resolution of our apparatus (i.e. $<\tau_{disp}> < 100$ ms).

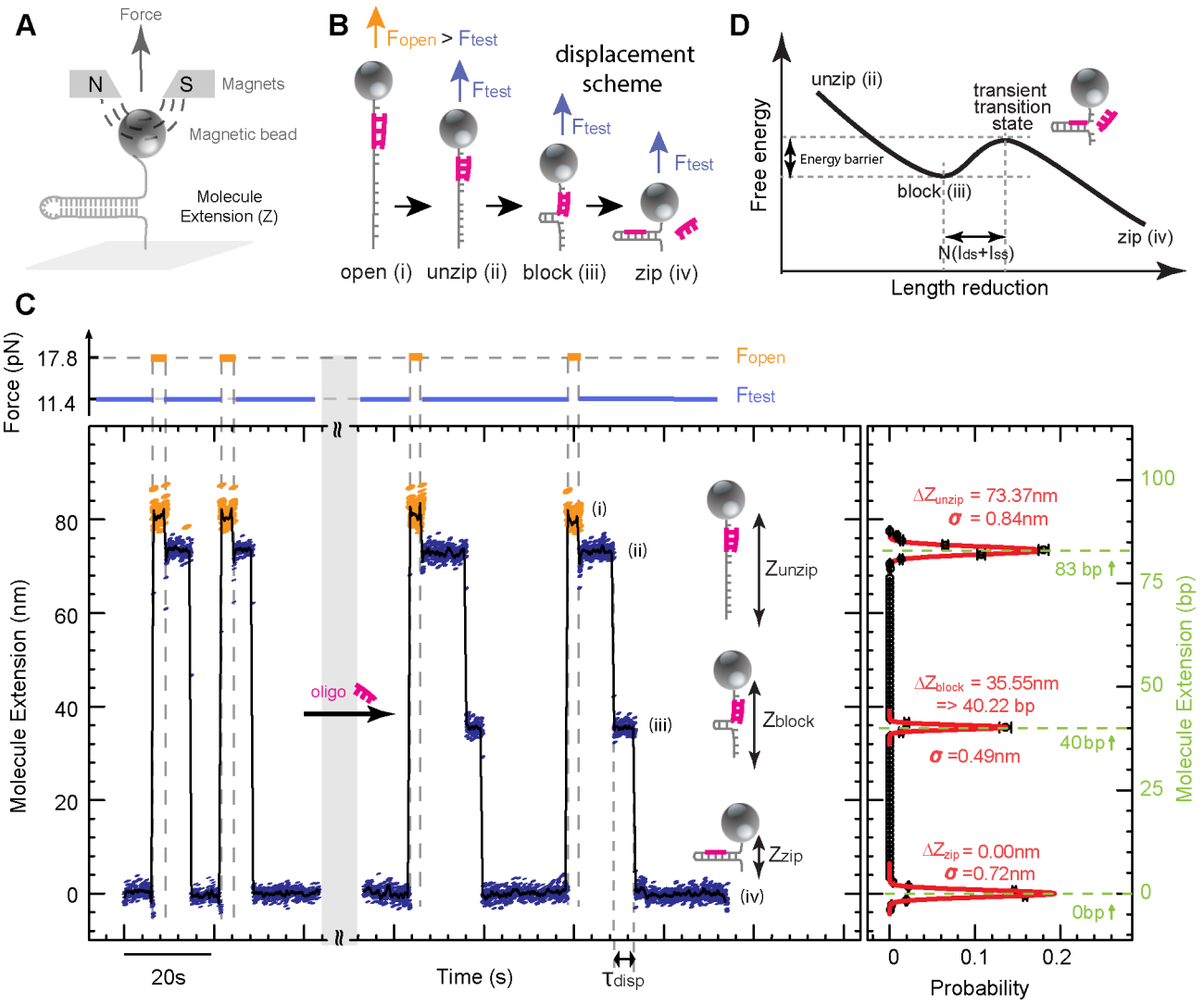


**Figure 1.** Detection of oligonucleotide-induced blockages during re-hybridization. (**A**) Schematic representation of the experimental set-up (6). (**B**) Schemes of the experimental process. Five different extension levels are expected: (i) $Z_{open}$ the fully unzipped hairpin at a force $F_{open}$ large enough (>15 pN) to open it, (ii) $Z_{unzip}$, the transient extension of the unzipped hairpin at a force $F_{test}$ too small (<12 pN) to prevent its re-hybridization, (iii) the partially rezipped hairpin blocked by an oligonucleotide at $Z_{block}$, the transition state, and (iv) the extension $Z_{zip}$ of a fully folded hairpin. (**C**) Left panel: Experimental traces of an 83 bp hairpin recorded at $F_{open}$ = 17.8 pN (orange) and $F_{test}$ = 11.4 pN (blue; see force trace at the top), marked as in (B). The black curve corresponds to a 1 s average of the raw data. Right panel: Histogram of blockages. The black curve represents the histogram of the number of blockages per cycle at a given extension of the hairpin upon re-hybridization at $F_{test}$: $\Delta Z = Z_{block} - Z_{zip}$ in nm on the left scale and base pairs on the right scale, obtained from a single hairpin. Gaussian fits to the data are shown in red. The variance of these fits ($\sigma \sim 1$ nm) defines the resolution of the apparatus. The roadblocks $Z_{block}$ is observed at the expected positions (green dashed line). Notice that reducing the force from $F_{open}$ to $F_{test}$ results in a slight change in the extension of the ssDNA, due to its elastic properties (Figure 1C and Supplementary Figure S5). (**D**) The scheme of energy landscape. The labelled (i)–(iv) status are corresponding to the ones shown in (B).

Interestingly while the position of destabilizing mismatches strongly affects $<\tau_{disp}>$, the effect of a stabilizing hybrid base pair (DNA–RNA, DNA–LNA, DNA–methylated DNA) is mostly position independent.

### The loop blocking assay: oligonucleotide binding to the hairpin apex

We now look into the 'dissociation' scheme with an experiment we call the loop blocking assay. The oligonucleotide, being at the hairpin apex, is not subject to the displacement by the fork (see Figure 4A). The oligo-hybrid inhibits refolding of the hairpin by sequestering its nucleation region. When the oligonucleotide spontaneously unbinds (*dissociation pathway*) after Figure 4A, the hairpin refolds (leading to a simple measure of $\tau_{off}$). At low forces, an alternative *encircling pathway* appears, with the hairpin nucleating and refolding in the back of the blocking oligonucleotide, Figure 4A.

Due to the increase in $<\tau_{off}>$ compared with $<\tau_{disp}>$ and the range of timescales that can be explored (typically between 0.1 and 300 s), the length of the oligonucleotides studied is quite narrow: 8 or 9 nucleotides. At 5–6 pN, a 9 nt oligonucleotide displays a mean dis-

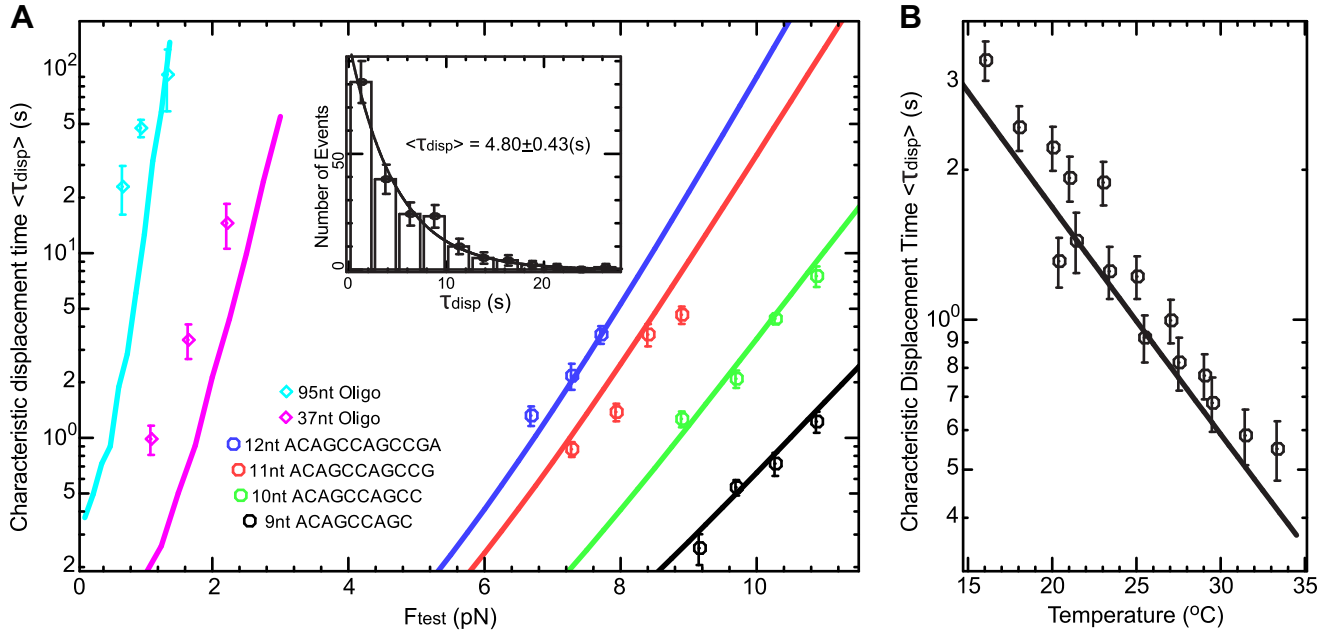


**Figure 2.** Influence of oligonucleotide length and temperature on the displacement time $<\tau_{disp}>$. (**A**) The displacement time versus oligonucleotide length in the fork blocking assay. (Insert) The histogram of the blocking time $\tau_{disp}$ displays a single exponential distribution with characteristic displacement time $<\tau_{disp}>$. $\tau_{disp}$ are obtained from ~200-fold/unfold hairpin cycles on the same molecule. The line is the prediction from a model of strand displacement (see Eq. 1). Points show the experimental evolution of $<\tau_{disp}>$ versus $F_{test}$ for oligonucleotides of length $N$ ($9 \leq N \leq 12$). In a simple picture, $<\tau_{disp}>$ varies exponentially with $F_{test}$. As a result, for a given hairpin, $<\tau_{disp}>$ can only be measured in a narrow force range. Adapting $F_{test}$ provides a way to study the hybridization over a large range of lengths, here $N$ varies from 9 to 95 nt (Supplementary Figure S2). The coloured continuous lines correspond to the predictions of the model described in the text. (**B**) Displacement time for the 10 nt oligonucleotide at a force $F_{test} = 8.5$ pN as a function of the temperature. Decreasing the temperature increases the oligonucleotide stability as expected from the model (continuous line).

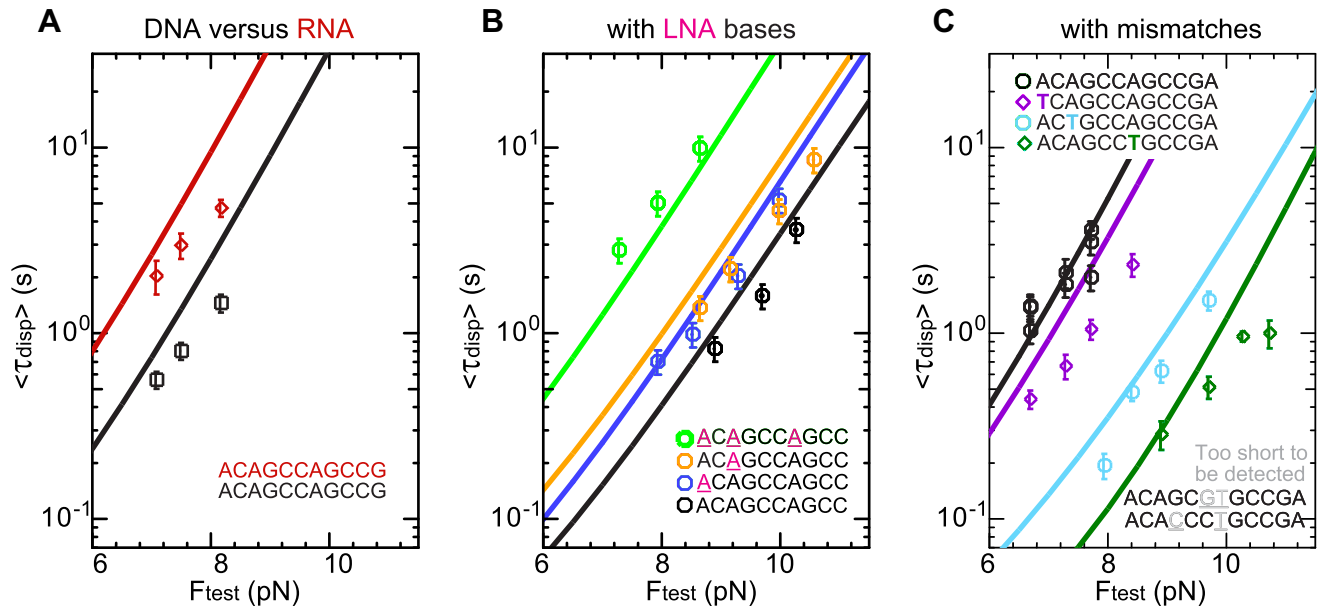


**Figure 3.** Influence of nucleotide types on the displacement time $<\tau_{disp}>$. (**A**, **B**) Increased binding stability induced by changing nucleotides from DNA to (A) RNA, (B) LNA. The continuous lines are predictions based on the model described in Methods: (A) for 11 nt RNA, the model fits the data by considering an increase of stability of $\Delta\Delta G = 1.1$ kcal/mol for each the 11 nt DNA–RNA oligonucleotide, and the prediction made using dinucleotide energy from overestimating the experimental results. (B) For 10 nt oligonucleotides with 1 or 3 LNA bases, the model fits the data with the following sequence dependent LNA–DNA increases in stability $\Delta\Delta G(AC) = -0.5$ (kcal/mol), $\Delta\Delta G(CA) = -0.1$ (kcal/mol), $\Delta\Delta G(AG) = -0.45$ (kcal/mol). The underlined base in the motif is a LNA (all full lines have been divided by 1.5 so that the pure DNA case fits properly). (**C**) Evolution of $<\tau_{disp}>$ versus mismatch position in an oligonucleotide having 12 nt. The blue points correspond to the original oligonucleotide without mismatches, and the other colours correspond to an oligonucleotide with a mismatch at the underlined position. The model fits the data with a pairing parameter due to mismatches caused by the substitution of an A with a T in the oligonucleotide $\Delta G(TC/TG) = 0.304$ (kcal/mol), $\Delta G(TG/TC) = -0.289$ (kcal/mol) and $\Delta G(CT/GT) = -0.289$ (kcal/mol). In agreement with the model, the displacement time of the oligonucleotides ACAGCGTCCCGA and ACACCCTGCCGA with two mismatches are too short to be detected.

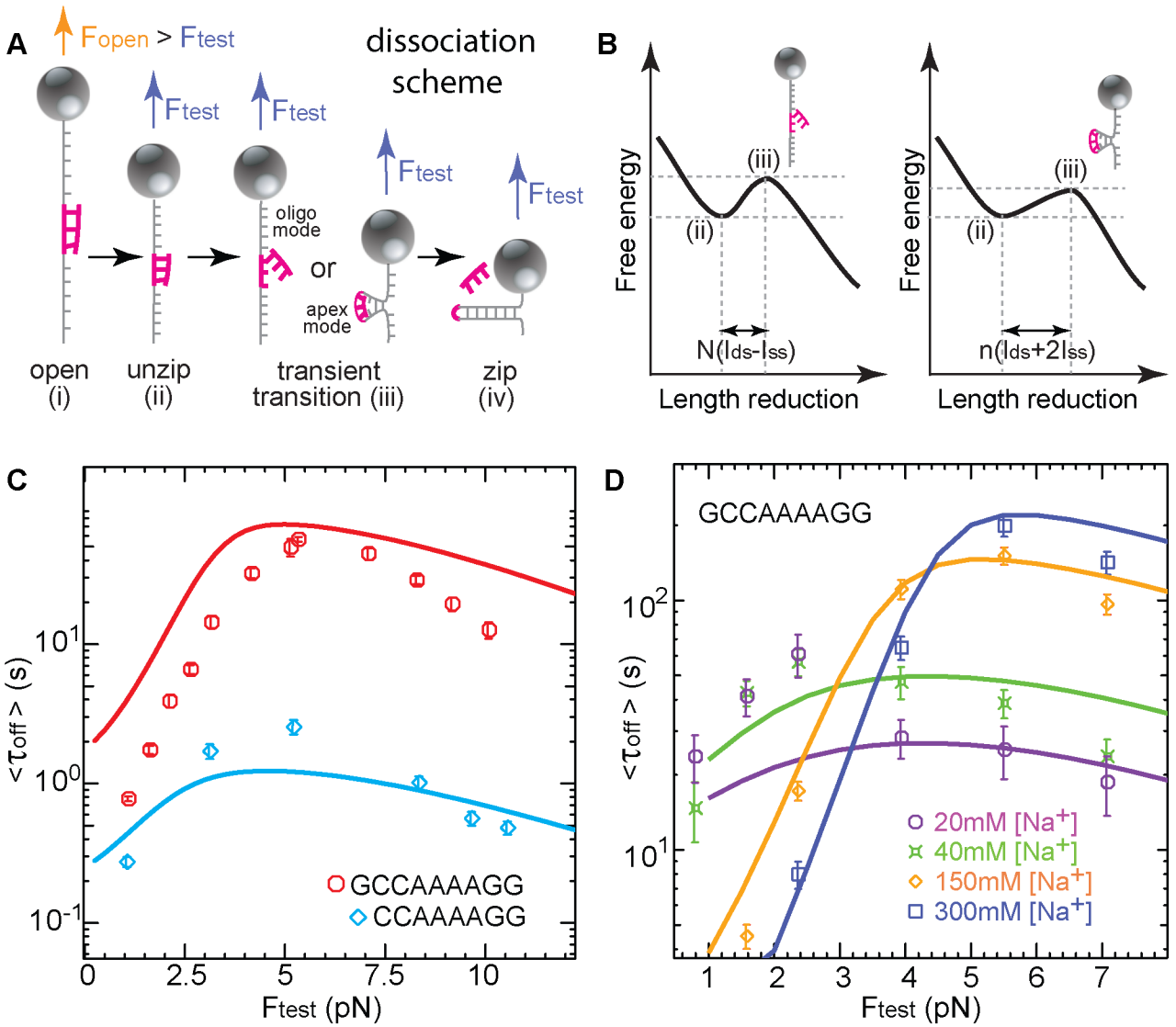


**Figure 4.** The oligonucleotide blocking time $\tau_{off}$ in the loop blocking assay versus $F_{test}$. (**A, B**) Schemes of the experimental process (A) and the energy landscape (B): (i) the hairpin is open, allowing the oligonucleotide hybridization at the apex of the hairpin. When this hybridization occurs, it transiently prevents the hairpin refolding (ii) for a time $\tau_{off}$. Two mechanisms are possible for the oligonucleotide release: at high force (iii) spontaneous detachment; at low force (iii) the hairpin refolds encircling the oligonucleotide, i.e. the two spontaneous dissociation pathways: 'oligo' and 'apex' mode. The final state (iv) corresponds to the hairpin refolded. (**C**) $<\tau_{off}>$ versus $F_{test}$ for an 8 nt (blue) and 9 nt (red) oligonucleotide blocking in the hairpin loop in Passivation Buffer ($T = 25°C$ with [NaCl] = 150 mM). (**D**) $<\tau_{off}>$ versus $F_{test}$ for the 9 nt oligonucleotide blocking in the hairpin loop in various salt concentrations. For both (C) and (D), full lines are predictions using the model in the main text without fork pressure. The energy barrier determining $<\tau_{off}>$ is dominated by the pairing energies and depends on the force through the change of extension between ssDNA and dsDNA.

sociation time $<\tau_{off}>$ twenty times longer than an 8 nt oligonucleotide, Figure 4C. We have studied the variation of $<\tau_{off}>$ with $F_{test}$ in various salts and temperature conditions. $<\tau_{off}>$ increases by a factor ~2 for a temperature decrease of only 3°C (see oligonucleotide GCCAAAAGG at 150 mM NaCl in Figure 4C at 25°C and Figure 4D at 22°C). Similarly, $<\tau_{off}>$ depends much more than $<\tau_{disp}>$ on salt concentrations: at high forces ($F > 5$ pN) the *dissociation pathway* leads to an increase of $<\tau_{off}>$ by almost an order of magnitude between 20 and 300 mM NaCl, while at low forces the *encircling pathway* leads to a decrease of $<\tau_{off}>$ by almost an order of magnitude between 20 and 300 mM NaCl.

### A model and a script predicting oligonucleotide displacement and dissociation

We modelled the displacement of an oligonucleotide by a closing dsDNA fork, in the blocking fork assay ('fork' mode), and its dissociation ('oligo' mode) or encirclement ('apex' mode) in the blocking loop assay. In the three cases, the process is described by the base by base opening/closing dynamics driven by thermal fluctuations (17,27,28). Opening/closing probabilities depend on elastic and base pairing energies (using the MeltingTemp.py script from BioPython 1.79) as described in Figure 5. Such a coarse-grained model is studied by both the Transition

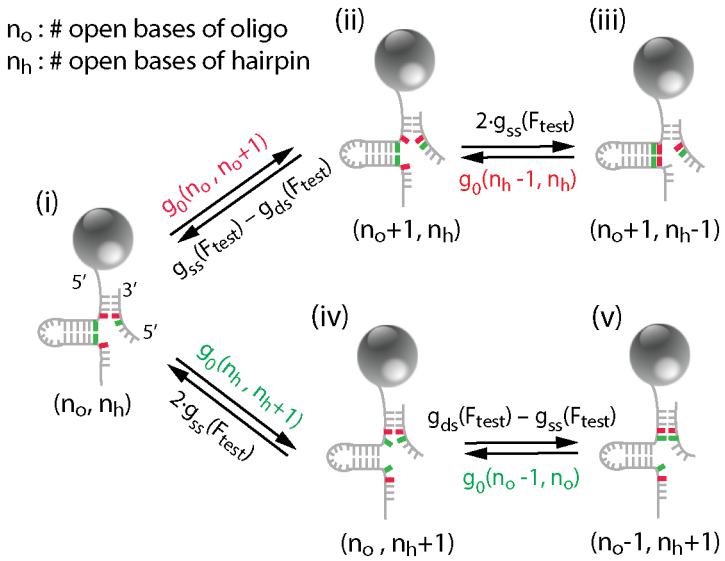


**Figure 5.** The transition elements and how to escape from a closing-blocked condition (i). Forward step: (ii) opening of the terminal base pair of the oligonucleotide followed by (iii) closing of the terminal base pair of the hairpin fork. Backward step: (iv) opening of the hairpin fork followed by (v) closing of the oligonucleotide. Note that the opening of a base pair of the oligonucleotide from (ii) and of the hairpin from (iv) are also possible, but the direct closing of the oligonucleotide from (iii) or of the hairpin fork from (v) is not possible. $g_{ss}(F_{test})$, and $g_{ds}(F_{test})$ are respectively the single-strand and double-strand elastic energies at the pulling force $F_{test}$. $g_o(n,n+1)$ are the zero-force base pairing energies which depend on the sequence (red or green bases) and include base-stacking effects. The opening and closing rates in the transition matrix are proportional to the exponent of the negative energy costs associated with the transitions indicated by the arrows.

Matrix approach (Supplementary note 1 and 2) and Monte-Carlo simulations (Supplementary note 1 and 3).

We provide a Python program corresponding to this last case which predicts $<\tau_{disp}>$ or $<\tau_{off}>$ for any sequence (with and without mismatches for DNA/DNA) and various salt conditions, forces, temperatures, and nucleotide types in the three modes (provide that the mismatch energy is known in BioPython).

The displacement ('fork' mode) is described by a scheme involving three fronts: both ends of the oligonucleotide experience peeling fluctuations, and the hairpin fork is the third front. In practice, the oligonucleotide bases are most of the time fully hybridized, but fluctuations can drive the transient opening of one base. When an oligonucleotide base transiently opens on the side of the closing fork, the fork can advance, preventing further closing of the oligonucleotide (Figure 5). Oligonucleotide displacement is mostly achieved by the fork, while unpeeling at the opposite end of the oligonucleotides detaches one or two bases at most in the complete process.

Each time the fork advances by one base, there is no net loss in pairing energy because the base pairing is exchanged between the oligonucleotide and the hairpin complementary strand. Thanks to this replacement mechanism, the displacement process is very fast compared to spontaneous dissociation. Indeed, it has an overall energetic cost only due to the shortening of the pulled hairpin strand under the force $F_{test}$. This activation barrier (see Figure 1D) explains several of our observations via an Arrhenius law: (i) the exponential distribution of the displacement times $<\tau_{disp}>$ (see Figure 2A (inset)), (ii) the increase in displacement time with the force $F_{test}$ and the oligonucleotide length and (iii) the ability to displace very long oligonucleotides by lowering $F_{test}$ (Figure 2A). Mismatches and base variants can also easily be taken into account by modifying the pairing energy in the replacement process (Figure 3).

The spontaneous dissociation pathway ('oligo' and 'apex' mode) in the loop blocking assay is described by an unpeeling process ('oligo' mode), which can be combined with encirclement ('apex' mode). Unpeeling engages the two ends of the oligonucleotide (21). At each step, the position of the first or the last hybridized base of the oligonucleotide has the possibility to unpeel or re-zip by one base. Owing to the difference in energy, the probability for a re-hybridization (which only costs the difference in the stretching energy at $F_{test}$ between double and single strand) is much higher than for unpeeling (which costs the energy of the base pairing). The unpeeling fronts stay most of the time close to the first and the last bases. Nevertheless, on some rare occasions, a series of unpeeling events occurs that leads to complete unbinding of the oligonucleotide.

As shown in Figure 4B and C, the large activation barrier due to unpairing (dissociation) explains the general behaviour of the experimental results at large forces and the great dependence of the displacement time on oligonucleotide length and sequence. To describe the rapid decrease of $<\tau_{off}>$ observed at low forces, we have added an encircling pathway to our model, which accounts for the possibility that a hairpin stem forms downstream of the oligonucleotide with a cost depending on the loop formation energy, resulting in the hairpin encircling the hybrid and displacing it.

As shown in Figure 4C and D, a model combining unpeeling and encircling ('apex' mode) in the transition matrix fits the data well. There is a crossover force between the two processes at about 5 pN depending on a model for the

elementary encircling rate (see methods and Supplementary note 2).

### Comparison of the experimental results with our model prediction

The coarse-grained description introduced here reproduces our experimental data with only a few adjustable parameters: $t_0$, an elementary time for each step (which sets the timescale for displacement) and λ, a salt correction factor; β and $t_u$ ($t_u = t_0\ 0.31^n$), the salt correction and elementary rate of encircling (Supplementary note 2). Note that while $t_0$ and λ are involved in all modes, $t_u$ and β are only required for the encircling mechanism occurring in the apex mode. We have used the pairing-energy parameters, from the literature (10–12,29–31), and suggested some corrections for the salt dependence and hybrid base pair interactions (DNA–RNA, DNA–LNA). We have set the parameters defining the elasticity of dsDNA and ssDNA from the literature and our measurements (23).

While Figures 2-4 present a comparison with the 'fork' and 'apex' modes, Figure 6 provides a comparison with experiments done by other groups (13,32,33) looking at simple oligonucleotide hybridization ('oligo' mode).

As can be seen on Figures 2 and 3, the agreement is good for $<\tau_{disp}>$ with a $t_0 = 2.5$ μs. The agreement is less good when using published $\Delta G$s (20,22) for RNA or LNA. The prediction of $\tau_{disp}$ is too high for RNA and too low for LNA. In the comparison of an oligonucleotide containing either all bases in RNA or in DNA, the predicted ΔΔG (30) reaches 1.58 $k_BT$ for 11 nt while our best fit is obtained for 1 $k_BT$ (0.6 kcal/mol). These energy differences lie within the errors of the nearest neighbour's parameters. The conclusion is the same for LNA. In fork mode, $<\tau_{disp}>$ does not depend significantly on the salt concentration but the binding probability increases proportionally with it. Our model predicts a mild increase of 50% of the displacement time when salt increases from 50 mM to 300 mM. We understand this effect since each base pair opening of the oligonucleotide is replaced by the same base pair closing in the hairpin.

In the 'apex' mode, $t_0 = 1$ μs, this replacement disappears and $<\tau_{off}>$ increases with the salt concentration (Figure 4D), as already reported (25). Our model fits this dependency well if we decrease the salt correction normally applied to ΔS when calculating the oligonucleotide melting temperature (10,19) by a factor ∼0.5 (Supplementary note 2). The need for this reduction is probably due to the difference in Manning condensation between dsDNA and ssDNA (34) (Supplementary note 2).

This salt effect is reinforced in the encircling pathway as the two ssDNA strands need to hybridize. We need to increase the salt correction on $\Delta S$ by a factor ∼2 (Supplementary note 2) to correctly fit the experimental data.

So far, we have discussed the $k_{off} = 1/\tau_{off}$ of an oligonucleotide, but we can also access the $k_{on}$: using the free energy of the base pairs and the normal salt correction ($\lambda = 1$), we compute the $\Delta G$ of the oligonucleotide and its $K_d = \exp(\Delta G/RT)$, then obtain $k_{on} = k_{off}/K_d$ (Figure 6). As a comparison, Zhang *et al.* (5) have measured the $k_{on}$ of a large set of 36 nt oligonucleotides and proposed a model predicting this $k_{on}$ but for a more complex hybridization situation than the two states model that is used here.

## DISCUSSION

Our assay allows measuring the kinetics of unbinding and replacement of an unlabeled oligonucleotide, in contrast with other approaches that use a fluorescently labelled oligonucleotide and thus are prone to limited observation time caused by photobleaching and to changes of binding affinity due to the interactions of fluorescent dyes with nucleic acids (35,36).

The oligonucleotide displacement described here is very similar to the replacement process of proteins bound to DNA by proteins in solutions (9), acting much faster than spontaneous dissociation (27,37). Here the replacement of the oligonucleotide is achieved by the DNA closing fork; there is then no dependence on the concentration of competing molecules in $<\tau_{disp}>$, but the set-up allows us to use the testing force as an essential control parameter.

The displacement model introduced here is an extension of the model for unzipping of DNA under force (37) but includes the competition of two unzipping processes on the same DNA. This model describes replacement at a base-pair scale which is more detailed than the strand displacement (38), the multi-strand simulator (39), or the single pathway models (40), but less detailed and computationally much less costly than molecular dynamics simulations (40,41) (see Supplementary note 1–3).

Our model provides a good agreement with our experiments taking into account that these times vary over several orders of magnitude since they depend exponentially upon the physical parameters involved.

When using an oligonucleotide complementary to a sequence in the hairpin apex, we have been able to investigate the unbinding time of the oligo-hybrid, a situation which has been investigated quite extensively using other means (mostly using fluorescently labelled oligonucleotides (13,32,33,42), though rarely with unlabeled ones (33,42)). We have used the same model to analyze these published experimental data. The agreement between the model predictions and the published data is reasonable as most of our predictions are within a factor of ∼4 of the experimental values. The most severe disagreements occur for long $\tau_{off}$ (>100 s) where the experimentally reported value is shorter than our prediction. That discrepancy could be attributed to photobleaching which affects the estimate of long $\tau_{off}$. The experimental data might also be affected by interactions between the fluorescent dyes and the DNA which may affect the hybridization free energies as reported in (36). Overall, our model provides a means to estimate the hybridization time of oligonucleotides to their template with and without mismatches, and it provides a solid foundation for the understanding of oligo-hybrid displacement by a receding fork, a situation of biological importance.

We have also observed that at low forces, nucleation of a hairpin in the back of a blocking oligonucleotide could account quantitatively for our observations. Such processes could play an important role in other situations where formation of a DNA bubble around an enzyme could mask its action, as in the unwinding of a DNA fork by a helicase (43) or the formation of an R-loop.

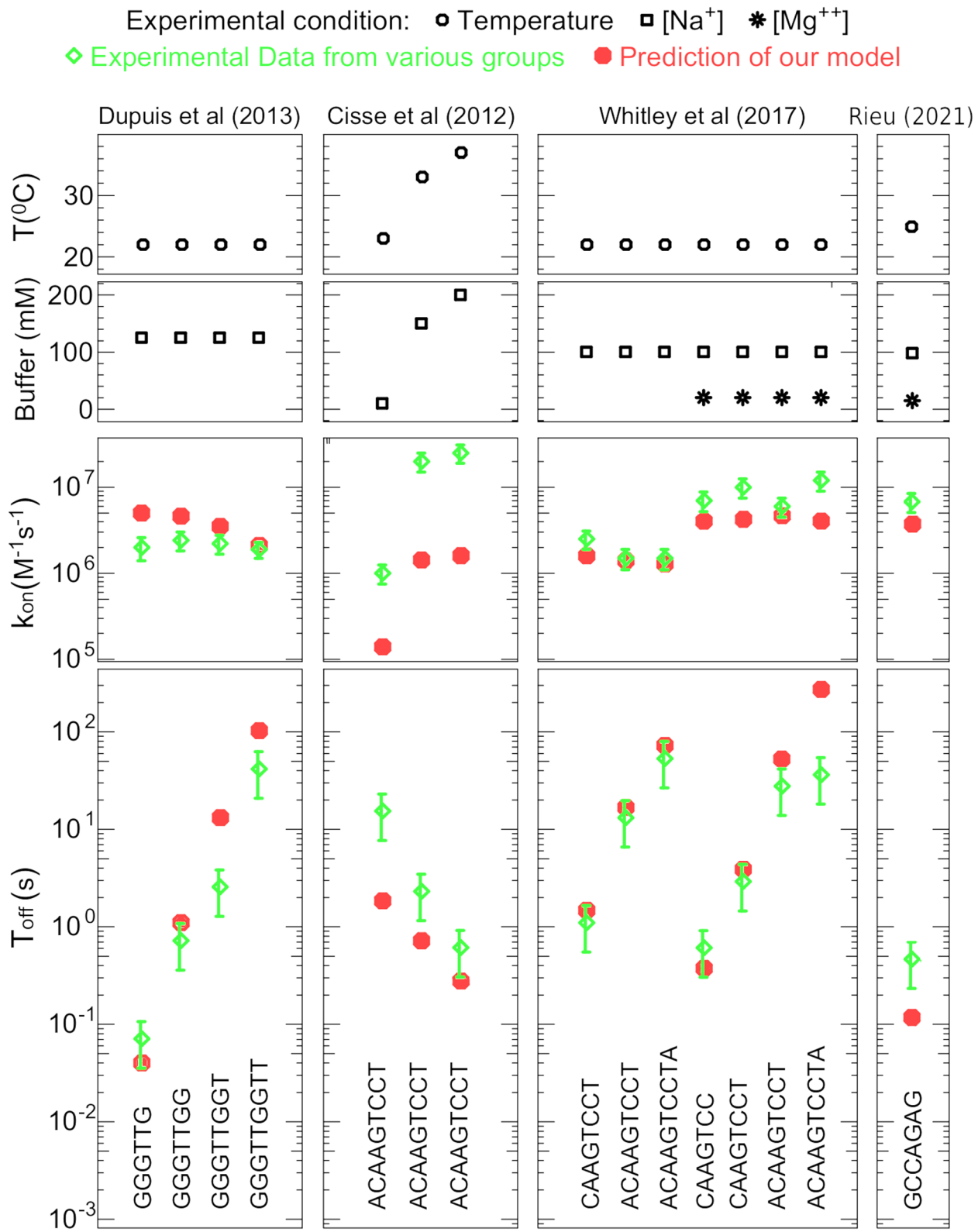


**Figure 6.** Comparison of oligonucleotide binding kinetics with experimental measurements done by various groups. Dupuis *et al.* (32), Cisse *et al.* (13), Whitley *et al.* (33) and Rieu *et al.* (42). All these measurements (excepted Rieu) are made using fluorescence which is limited by photobleaching. As shown in the figure, our model has good agreement with all the experimental data across four groups, especially the duration of $\tau_{off}$.

The sensitivity of $<\tau_{off}>$ to the nature and position of mismatches has also been reported in a pure hybridization assay (6). When using the present assay to probe a DNA sequence, such sensitivity could be used to detect 'single nucleotide polymorphisms' (6,44).

Our work provides a tool to predict the dissociation time $\tau_{off}$ of an oligonucleotide which should be useful for many applications. The present accuracy is reasonable, but there is room for improvements by adjusting the various parameters for which we have proposed starting values; this could be done by using a more elaborate ssDNA elasticity model (24,25) and by using systematic label-free measurement as proposed in (42).

There are some other published experimental approaches that have also been carried out on unlabelled oligonucleotides to understand DNA hybridization kinetics. For example, temperature jumps experiments using infrared spectroscopy coupled with computational modeling show that DNA hybridization and dehybridization depend on their length (45) and sequence (46,47), which establish a link between thermodynamics and kinetics of the processes and provide more insight into the dynamical transition states besides the canonical two-state model. Also, studies of bulk oligonucleotide duplexes in solution using stopped-flow experiments draw the distinctions between DNA association and dissociation kinetics and analyze the influence of ionic conditions as well as GC contents (48) on the processes. Similarly, bulk experiments using ultraviolet absorbance show that inherent DNA secondary structures decrease intermolecular hybridization kinetic rate, and DNA surface hybridization is 20–40-fold slower than in solution (49). However, those works were performed in bulk, missing single molecule level readout.

Advances in single-molecule works include experiments inferring DNA hybridization kinetics through measuring real-time conductance during DNA hybridization to immobilized probes on the Au (111) (50) or graphene (51) sensor surface. Both findings support concentration-dependent DNA hybridization kinetics, and the latter can resolve single-base mismatches. However, those works focus on DNA hybridization in terms of dissociation only. Here, we also quantitatively study the dynamics process of DNA oligo displacement by the hairpin fork and highlight their differences from DNA dissociation, with single base-pair and micro-second resolution in a real-time and high-throughput fashion.

The novel assay proposed here provides insight into the displacement of DNA/DNA hybrids by a complementary strand, a situation encountered both in vivo, such as in transcription pausing and replication arrest, and in vitro during DNA-origami formation (4) and the study of DNA walkers and CRISPR (7). Using this approach, we have already successfully achieved DNA sequencing and identification at the single molecule level (6). We provide here a model and software allowing prediction of the oligonucleotide displacement time and thus a way to optimize probes for these applications. We also demonstrate the validity of the model by measuring the oligonucleotide unbinding kinetics. As a further application, the novel assay combined with the replacement model can be used to better determine base-pair parameters and end effects in pairing energies.

## DATA AVAILABILITY

Oligonucleotide sequences are listed in the figures and/or the section of material and methods. Other data presented in this study is available upon reasonable request to the corresponding authors.

## SUPPLEMENTARY DATA

Supplementary Data are available at NAR Online.

## ACKNOWLEDGEMENTS

We thank M. Rieu, T. Loveless, B. Ducos, C. Andre, for useful comments on the manuscript and R. Monasson for helpful discussions on the modelling.
*Author contributions*: Conceptualization: F.D., S.C., M.M., D.B., J.A., V.C. Methodology: F.D., S.C., M.M., D.B., J.A., V.C. Investigation: F.D., S.C., S.R., M.M., M.M.S., V.C. Writing original draft: F.D., S.C., D.B., J.A., V.C. Writing review & editing: F.D., T.N., V.C.

## FUNDING

Schlumberger Foundation (to F.D.); ERC [Magreps 267 862 to V.C.]; Human Frontier Science Program [RGP003/2007 to V.C.]; Fondation Pierre-Gilles de Gennes [FPGG032 to V.C.]; Centre National de la Recherche Scientifique (to V.C.); Spanish Research Council grant [PID2019-111148GB-100 to M.M.]; Spanish Ramon y Cajal programme of MICINN [to M.M.]; NIH Director's New Innovator Award [1DP2GM149554]; University of California-Irvine (to F.D.); funding support for M.M.S. and DNA hairpin synthesis was provided by a Human Frontier Science Program grant [RGP003/2007]; US National Institutes of Health grant [GM013306 to S.J.B.]. Funding for open access charge: NIH Director's New Innovator Award [1DP2GM149554 to F.D.].
*Conflict of interest statement.* V.C., D.B. and J.A. are co-founders of Depixus, a company that will benefit from the work described here.

## REFERENCES

1. Tadigotla,V.R., O Maoiléidigh,D., Sengupta,A.M., Epshtein,V., Ebright,R.H., Nudler,E. and Ruckenstein,A.E. (2006) Thermodynamic and kinetic modeling of transcriptional pausing. *Proc. Natl. Acad. Sci. U.S.A.*, **103**, 4439–4444.
2. Dirks,R.M. and Pierce,N.A. (2004) Triggered amplification by hybridization chain reaction. *Proc. Natl. Acad. Sci. U.S.A.*, **101**, 15275–15278.
3. Shin,J.-S. and Pierce,N.A. (2004) A synthetic DNA walker for molecular transport. *J. Am. Chem. Soc.*, **126**, 10834–10835.
4. Winfree,E., Liu,F., Wenzler,L.A. and Seeman,N.C. (1998) Design and self-assembly of two-dimensional DNA crystals. *Nature*, **394**, 539–544.
5. Zhang,D.Y. and Seelig,G. (2011) Dynamic DNA nanotechnology using strand-displacement reactions. *Nat. Chem.*, **3**, 103–113.
6. Ding,F., Manosas,M., Spiering,M.M., Benkovic,S.J., Bensimon,D., Allemand,J.-F. and Croquette,V. (2012) Single-molecule mechanical identification and sequencing. *Nat. Methods*, **9**, 367–372.
7. Cong,L., Ran,F.A., Cox,D., Lin,S., Barretto,R., Habib,N., Hsu,P.D., Wu,X., Jiang,W., Marraffini,L.A. *et al.* (2013) Multiplex genome engineering using CRISPR/Cas systems. *Science*, **339**, 819–823.

8. Graham,J.S., Johnson,R.C. and Marko,J.F. (2011) Concentration-dependent exchange accelerates turnover of proteins bound to double-stranded DNA. *Nucleic Acids Res.*, **39**, 2249–2259.
9. Paramanathan,T., Reeves,D., Friedman,L.J., Kondev,J. and Gelles,J. (2014) A general mechanism for competitor-induced dissociation of molecular complexes. *Nat. Commun.*, **5**, 5207.
10. SantaLucia,J. Jr (1998) A unified view of polymer, dumbbell, and oligonucleotide DNA nearest-neighbor thermodynamics. *Proc. Natl. Acad. Sci. U.S.A.*, **95**, 1460–1465.
11. Allawi,H.T. and SantaLucia,J. Jr (1998) Nearest-neighbor thermodynamics of internal A.C mismatches in DNA: sequence dependence and pH effects. *Biochemistry*, **37**, 9435–9444.
12. Allawi,H.T. and SantaLucia,J. Jr (1998) Nearest neighbor thermodynamic parameters for internal G.A mismatches in DNA. *Biochemistry*, **37**, 2170–2179.
13. Cisse,I.I., Kim,H. and Ha,T. (2012) A rule of seven in watson-crick base-pairing of mismatched sequences. *Nat. Struct. Mol. Biol.*, **19**, 623–627.
14. Lionnet,T., Spiering,M.M., Benkovic,S.J., Bensimon,D. and Croquette,V. (2007) Real-time observation of bacteriophage T4 gp41 helicase reveals an unwinding mechanism. *Proc. Natl. Acad. Sci. U.S.A.*, **104**, 19790–19795.
15. Manosas,M., Spiering,M.M., Zhuang,Z., Benkovic,S.J. and Croquette,V. (2009) Coupling DNA unwinding activity with primer synthesis in the bacteriophage T4 primosome. *Nat. Chem. Biol.*, **5**, 904–912.
16. Odijk,T. (1995) Stiff chains and filaments under tension. *Macromolecules*, **28**, 7016–7018.
17. Cocco,S., Marko,J.F. and Monasson,R. (2003) Slow nucleic acid unzipping kinetics from sequence-defined barriers. *Eur. Phys. J. E Soft Matter*, **10**, 153–161.
18. SantaLucia,J. Jr and Hicks,D. (2004) The thermodynamics of DNA structural motifs. *Annu. Rev. Biophys. Biomol. Struct.*, **33**, 415–440.
19. Zuker,M. (2003) Mfold web server for nucleic acid folding and hybridization prediction. *Nucleic Acids Res.*, **31**, 3406–3415.
20. Owczarzy,R., You,Y., Groth,C.L. and Tataurov,A.V. (2011) Stability and mismatch discrimination of locked nucleic acid-DNA duplexes. *Biochemistry*, **50**, 9352–9367.
21. Cocco,S., Yan,J., Léger,J.-F., Chatenay,D. and Marko,J.F. (2004) Overstretching and force-driven strand separation of double-helix DNA. *Phys. Rev. E Stat. Nonlin. Soft Matter Phys.*, **70**, 011910.
22. Sugimoto,N., Nakano,S., Katoh,M., Matsumura,A., Nakamuta,H., Ohmichi,T., Yoneyama,M. and Sasaki,M. (1995) Thermodynamic parameters to predict stability of RNA/DNA hybrid duplexes. *Biochemistry*, **34**, 11211–11216.
23. Manosas,M., Perumal,S.K., Croquette,V. and Benkovic,S.J. (2012) Direct observation of stalled fork restart via fork regression in the T4 replication system. *Science*, **338**, 1217–1220.
24. Jacobson,D.R., McIntosh,D.B., Stevens,M.J., Rubinstein,M. and Saleh,O.A. (2017) Single-stranded nucleic acid elasticity arises from internal electrostatic tension. *Proc. Natl. Acad. Sci. U.S.A.*, **114**, 5095–5100.
25. Viader-Godoy,X., Pulido,C.R., Ibarra,B., Manosas,M. and Ritort,F. (2021) Cooperativity-dependent folding of single-stranded dNA. *Phys. Rev. X.*, **11**, 031037.
26. Liu,J.-P., Drungowski,M., Nyársik,L., Schwartz,R., Lehrach,H., Herwig,R. and Janitz,M. (2007) Oligonucleotide fingerprinting of arrayed genomic DNA sequences using LNA-modified hybridization probes. *Comb. Chem. High Throughput Screen.*, **10**, 269–276.
27. Cocco,S., Marko,J.F. and Monasson,R. (2014) Stochastic ratchet mechanisms for replacement of proteins bound to DNA. *Phys. Rev. Lett.*, **112**, 238101.
28. Machinek,R.R.F., Ouldridge,T.E., Haley,N.E.C., Bath,J. and Turberfield,A.J. (2014) Programmable energy landscapes for kinetic control of DNA strand displacement. *Nat. Commun.*, **5**, 5324.
29. Allawi,H.T. and SantaLucia,J. Jr (1997) Thermodynamics and NMR of internal G.T mismatches in DNA. *Biochemistry*, **36**, 10581–10594.
30. Watkins,N.E. Jr and SantaLucia,J. Jr (2005) Nearest-neighbor thermodynamics of deoxyinosine pairs in DNA duplexes. *Nucleic Acids Res.*, **33**, 6258–6267.
31. Peyret,N., Seneviratne,P.A., Allawi,H.T. and SantaLucia,J. Jr (1999) Nearest-neighbor thermodynamics and NMR of DNA sequences with internal A.A, C.C, G.G, and T.T mismatches. *Biochemistry*, **38**, 3468–3477.
32. Dupuis,N.F., Holmstrom,E.D. and Nesbitt,D.J. (2013) Single-molecule kinetics reveal cation-promoted DNA duplex formation through ordering of single-stranded helices. *Biophys. J.*, **105**, 756–766.
33. Whitley,K.D., Comstock,M.J. and Chemla,Y.R. (2017) Elasticity of the transition state for oligonucleotide hybridization. *Nucleic Acids Res.*, **45**, 547–555.
34. Vuletić,T., Babić,S.D., Grgičin,D., Aumiler,D., Rädler,J., Livolant,F. and Tomić,S. (2011) Manning free counterion fraction for a rodlike polyion: aqueous solutions of short DNA fragments in presence of very low added salt. *Phys. Rev. E Stat. Nonlin. Soft Matter Phys.*, **83**, 041803.
35. Biebricher,A.S., Heller,I., Roijmans,R.F.H., Hoekstra,T.P., Peterman,E.J.G. and Wuite,G.J.L. (2015) The impact of DNA intercalators on DNA and DNA-processing enzymes elucidated through force-dependent binding kinetics. *Nat. Commun.*, **6**, 7304.
36. Moreira,B.G., You,Y. and Owczarzy,R. (2015) Cy3 and Cy5 dyes attached to oligonucleotide terminus stabilize DNA duplexes: predictive thermodynamic model. *Biophys. Chem.*, **198**, 36–44.
37. Woodside,M.T., Behnke-Parks,W.M., Larizadeh,K., Travers,K., Herschlag,D. and Block,S.M. (2006) Nanomechanical measurements of the sequence-dependent folding landscapes of single nucleic acid hairpins. *Proc. Natl. Acad. Sci. U.S.A.*, **103**, 6190–6195.
38. Reynaldo,L.P., Vologodskii,A.V., Neri,B.P. and Lyamichev,V.I. (2000) The kinetics of oligonucleotide replacements. *J. Mol. Biol.*, **297**, 511–520.
39. Zhang,D.Y. and Winfree,E. (2009) Control of DNA strand displacement kinetics using toehold exchange. *J. Am. Chem. Soc.*, **131**, 17303–17314.
40. Srinivas,N., Ouldridge,T.E., Sulc,P., Schaeffer,J.M., Yurke,B., Louis,A.A., Doye,J.P.K. and Winfree,E. (2013) On the biophysics and kinetics of toehold-mediated DNA strand displacement. *Nucleic Acids Res.*, **41**, 10641–10658.
41. Liu,H., Hong,F., Smith,F., Goertz,J., Ouldridge,T., Stevens,M.M., Yan,H. and Šulc,P. (2021) Kinetics of RNA and RNA:DNA hybrid strand displacement. *ACS Synth. Biol.*, **10**, 3066–3073.
42. Rieu,M., Valle-Orero,J., Ducos,B., Allemand,J.-F. and Croquette,V. (2021) Single-molecule kinetic locking allows fluorescence-free quantification of protein/nucleic-acid binding. *Commun. Biol.*, **4**, 1083.
43. Fiorini,F., Bagchi,D., Le Hir,H. and Croquette,V. (2015) Human upf1 is a highly processive RNA helicase and translocase with RNP remodelling activities. *Nat. Commun.*, **6**, 7581.
44. Tang,W., Zhong,W., Tan,Y., Wang,G.A., Li,F. and Liu,Y. (2020) DNA strand displacement reaction: a powerful tool for discriminating single nucleotide variants. *Top. Curr. Chem. (J)*, **378**, 10.
45. Menssen,R.J. and Tokmakoff,A. (2019) Length-dependent melting kinetics of short DNA oligonucleotides using temperature-jump IR spectroscopy. *J. Phys. Chem. B*, **123**, 756–767.
46. Sanstead,P.J., Stevenson,P. and Tokmakoff,A. (2016) Sequence-dependent mechanism of DNA oligonucleotide dehybridization resolved through infrared spectroscopy. *J. Am. Chem. Soc.*, **138**, 11792–11801.
47. Jones,M.S., Ashwood,B., Tokmakoff,A. and Ferguson,A.L. (2021) Determining sequence-dependent DNA oligonucleotide hybridization and dehybridization mechanisms using coarse-grained molecular simulation, markov state models, and infrared spectroscopy. *J. Am. Chem. Soc.*, **143**, 17395–17411.
48. Rejali,N.A., Ye,F.D., Zuiter,A.M., Keller,C.C. and Wittwer,C.T. (2021) Nearest-neighbour transition-state analysis for nucleic acid kinetics. *Nucleic Acids Res.*, **49**, 4574–4585.
49. Gao,Y., Wolf,L.K. and Georgiadis,R.M. (2006) Secondary structure effects on DNA hybridization kinetics: a solution versus surface comparison. *Nucleic Acids Res.*, **34**, 3370–3377.
50. Harashima,T., Hasegawa,Y., Kaneko,S., Jono,Y., Fujii,S., Kiguchi,M. and Nishino,T. (2020) Elementary processes of DNA surface hybridization resolved by single-molecule kinetics: implication for macroscopic device performance. *Chem. Sci.*, **12**, 2217–2224.
51. Xu,S., Zhan,J., Man,B., Jiang,S., Yue,W., Gao,S., Guo,C., Liu,H., Li,Z., Wang,J. *et al.* (2017) Real-time reliable determination of binding kinetics of DNA hybridization using a multi-channel graphene biosensor. *Nat. Commun.*, **8**, 14902.